Short-range interference effect in the diffusion of light in random media

Sakae Kawato,* Toshiaki Hattori, Tadashi Takemori, and Hiroki Nakatsuka
Institute of Applied Physics, University of Tsukuba, Tsukuba, Ibaraki 305-8573, Japan
(Received 23 January 1998)

We study the interference effect of multiply scattered waves in the diffusive light propagation in random media. We take porous glass samples of various pore radii a as an example of random media, and measure the transport mean free path l^* and the diffusion constant D for various light wavelengths λ over a wide range of the size parameter $a/\lambda = 0.05$–0.85. A crossover is observed from the Rayleigh scattering region to the geometrical optics region. The transport velocity $v_E = 3D/l^*$ determined from the data is found to decrease monotonically with a/λ, falling well below the light velocity in glass. We also present a framework of theoretical analysis of wave energy diffusion in a most general setting, taking explicit account of the broadening of light dispersion and paying attention to the requirement of Ward-Takahashi identity. We calculate diffusion parameters as functions of a/λ for a model of spatially fluctuating dielectric constant, using two types of self-consistent scattering approximation to the self-energy and the scattering kernel. Comparison of the experiment against the calculation with and without interference terms of multiple scattering reveals the importance of short-range interference effects in the diffusive propagation of light. [S0163-1829(98)07133-1]

I. INTRODUCTION

Propagation of classical waves in random media has been a subject of investigation for quite some time. [1–3] It has long been observed that, in a wide range of cases, the propagation of energy over a long distance and over a long time is diffusive.[4] Examples include light propagation in the atmospheric cloud[4] and transmission of radio waves through a cloud of interstellar objects in space.[5] Electronic conduction through a resistor may also be put in the same context if one assumes a noninteracting Fermi fluid and solves the Schrödinger equation for the electronic wave function in a random potential.[6] In all such cases, long-range propagation is well described by a diffusion equation with a definite diffusion constant. One might then be tempted to construct a picture of energy diffusion in terms of the diffusion of particles which travel at a certain speed to undergo a series of collisions with pointlike scattering centers. A standard theory of such diffusion involves quantities such as transport mean free path l^* and transport velocity v_E, which are related to the diffusion constant D by $D = \frac{1}{3} v_E l^*$.[7,8] However, such a theory is so firmly based on the picture of diffusing classical particles, it does not readily yield to an interpretation in terms of the underlying wave propagation. The scattering cross section of individual scatterers may be determined in the wave picture to obtain l^*, and the wave propagation speed v_E may be determined from the energy propagation speed in the free space. But once these parameters are determined, one carries over to the particle picture and assumes that the wave nature is not manifest over a spatial distance beyond l^*.

However, the wave nature reappears beyond distances over l^* if the scattering is strong enough to satisfy the Ioffe-Regel criterion[9] $l^*/\lambda \lesssim 1/(2\pi)$, where λ is the wavelength of the propagating wave. Then the interference between multiply scattered waves is no longer negligible over long distances, and a linear wave can localize and cease to propagate diffusively.[10] This so-called Anderson localization was formulated for the Schrödinger equation for an electron in a random potential. However, the mathematical framework is general enough to be applicable to any form of linear wave equation, and wave localization has now been predicted for a wide range of systems from electromagnetic waves in a random dielectric medium [11–13] to sound waves in a nonuniform material.[14–16] Despite numerous attempts to realize localization of a classical wave, a conclusive demonstration has proved difficult. However, the observation of a precursor effect in the form of enhanced backscattering of light from disordered media[17–19] gave a clear demonstration of the existence of interference effects over long spatial distances. Investigation into the long-range interference effects has been intensively pursued ever since,[2,3,20,21] and an observation of a strong evidence of localization of light in GaAs powder was reported quite recently.[22]

Such developments, on the other hand, have given a renewed impetus also to the investigation into the nature of diffusive propagation of classical waves, especially to the effort to construct a full description of energy diffusion in terms of wave propagation. The diffusive behavior of energy propagation is a general phenomenon that is observed in a wide variety of random media. The scatterers may be particles of a finite size as in the case of polystyrene spheres suspended in water.[23] Porous glass, on the other hand, is a block of glass permeated by a random network of fine pores. One would have achieved a good understanding of the phenomenon of wave diffusion if one could calculate diffusion parameters such as l^*, D, and v_E from the knowledge of the microscopic structure of the random medium. However, it has been recognized that the definition of such parameters in the wave picture is far from trivial.[3,20,24] For example, it has been pointed out that in the case of light scattering by dielectric spheres of a finite size, the multiple scattering in and around each individual sphere results in a dwell time which slows down the propagation speed v_E considerably.[24–27] This was put forward as a possible explanation of the experimental results that the velocity v_E determined from the measurement of D and l^* very often came out smaller than the light

velocity either in the host material or inside the dielectric scatterer.[25] This fact indicates the importance of the interference effect of multiple scattering even in the diffusive regime well away from the Ioffe-Regel criterion.

So far, the theory of multiple light scattering is established only in the weak scattering limit and in the dilute limit of scatterer concentration. A commonly used treatment in the literature is the independent scattering approximation (ISA), which takes into account the wave interference in obtaining the scattering amplitude of individual scatterers but otherwise treats the propagation of light as the diffusion of classical particles.[3] In an ISA treatment, shell approximation is often implicitly used, where a definite dispersion relation is assumed in the material. This enables one to define without ambiguity such quantities as phase velocity and group velocity. Such a treatment is valid when the scatterer density is low, and gives indeed a good account of the energy diffusion under appropriate circumstances.[24–26] However, the diffusive behavior is not confined to such limiting cases but is widely observed even in cases of high scatterer concentration and large scattering amplitude, as long as the scattering mean free path l is longer than λ. Interference then takes place not only around individual scatterers but between different scatterers as well. For a fixed frequency, the wave vector is distributed over a width $\sim 2\pi/l$, so that there is a broadening of the dispersion relation. If the broadening cannot be ignored compared to $2\pi/\lambda$, the definition of such quantities as l^* and v_E is no longer straightforward. One is then in need of a consistent framework of description which goes beyond the shell approximation or the ISA, and which takes explicit account of the interference effect of multiple scattering. While wave interference around individual scattering centers results in a reduction of v_E in the framework of ISA, a full treatment of wave interference between different scatterers in a broader framework should affect all diffusion parameters D, l^*, and v_E.

Our aim is to establish a general description of light diffusion that is applicable to a wide variety of random media by taking into account the wave nature of light. In this paper, we address the problem on both experimental and theoretical fronts. Experimentally, we investigated light propagation in porous glass and measured transport mean free path l^*, diffusion constant D, and transport velocity v_E over a wide continuous range of the size parameter a/λ with a being the radius of the pores and λ being the wavelength of the incident light in vacuum. The result is analyzed in a theoretical framework that is general enough to encompass a wide variety of situations where light diffusion is observed. We compare model calculations with the experiment to elucidate the interference effect of multiple scattering in wave diffusion.

II. EXPERIMENTAL STUDY OF MULTIPLE SCATTERING OF LIGHT IN POROUS GLASS

We measured the transport mean free path l^* and the diffusion constant D of light in porous glass by measuring the transmission spectra and the temporal intensity profile of light pulses transmitted through the sample plates. The transport velocity v_E was obtained from D and l^* using the relation $D=v_E l^*/3$.

In the experiment of multiple scattering of light in random media, the key features required of the target sample are (1) well-characterized spatial structure, (2) high contrast of refractive index between the host and the scatterers, and (3) low light absorption. Commercially available porous silica glass provides an optimal choice for this purpose, since the pore radius is controlled to an accuracy of $\pm 10\%$ about its mean value, the volume fraction of the pores can be measured with precision, the contrast in refractive index is 1.5 for glass against 1.0 for air/vacuum, and glass has minimal absorption in the visible range of λ.[28] We used four porous glass plates [Asahi Glass, MPG-AM(S)] which we label A (mean pore radius $a=0.15$ μm, volume fraction of pores $f=0.53$), B ($a=0.275$ μm, $f=0.50$), C ($a=0.35$ μm, $f=0.49$) and D ($a=0.50$ μm, $f=0.48$), all of which were 0.5 mm thick.

Porous glass is an efficient adsorbent, so that, if exposed to atmosphere, it adsorbs a large number of OH groups and water molecules along with some other molecules on the pore surface. The OH group has weak absorption peaks in the visible region and a few stronger absorption peaks in the near-infrared region.[29] In order to eliminate the absorption, the porous glass plates were first treated chemically to remove OH groups and water. The procedure was as follows:[30]

(1) Boil the sample in oxygenated water for about 30 min, dry it by heating, and let it cool to room temperature.

(2) Soak the sample in 30% NH_4F_{aq} for 20 min, and then wash out the excess NH_4F.

(3) Bake the sample at 110 °C for 10 min, and let it cool down to room temperature.

(4) Soak the sample in 1N-HNO_3 to fix the fluorine onto the surface.

(5) After baking again at 110 °C for 15 min, put the sample in a vacuum cell.

(6) Heat the cell gently over a period of 30 min to bring the temperature up to 400 °C, and hold the temperature for 12 h.

In porous glass, a randomly connected network of pores permeates the glass, taking up as much as 50% of the total volume. The scatterer configuration is therefore far removed from that of sparsely distributed random scatterers which is often taken as a model of a random medium.

A. Transmission spectrum and transport mean free path

When the light propagation is diffusive, the transmittance T through a plate of random medium of thickness L is given by

$$T=\frac{z_p+z_0}{L+2z_0}, \tag{2.1}$$

according to the transport theory of diffusion.[31] It is assumed here that L is much larger than the transport mean free path l^*. The penetration depth z_p and the virtual extrapolation depth z_0 are both quantities proportional to l^*, with the proportionality coefficients varying to a small degree according to the method of estimation.[7,8,25] Employing the widely accepted values $z_p=l^*$ and $z_0=0.71l^*$, Eq. (2.1) can be used to obtain l^* from the transmittance T. By measuring the transmission spectra of the porous glass plates, we obtained the transport mean free path l^* over a wide range of λ.

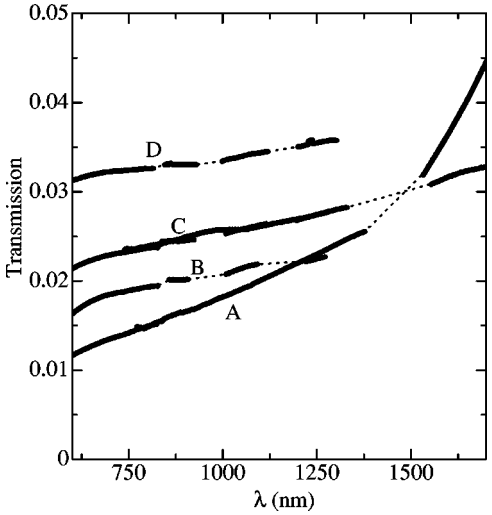

FIG. 1. Transmission spectra (bold curves) of porous glass plates A, B, C, and D. The pore radii are 0.15 μm (A), 0.275 μm (B), 0.35 μm (C), and 0.50 μm (D). The volume fraction of pores is 0.5, and λ is the wavelength of light in air.

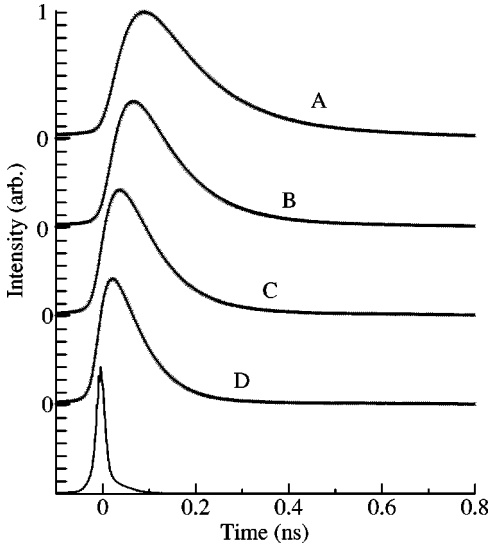

FIG. 3. Temporal intensity profile of the light pulse transmitted through samples A–D. The measured profile for the incident pulse is shown at the bottom.

The measured spectra for the four glass plates (A, B, C, and D) are shown in Fig. 1. We have omitted the data in the regions of known absorption peaks of OH groups and water molecules, since the raw data showed small dips that were clearly ascribable to the residual OH groups and water molecules on the pore surface. Figure 2 shows the normalized transport mean free path l^*/λ as a function of size parameter a/λ. In the figure we also show the ISA calculations using the Mie scattering amplitude for spherical holes of radius a in glass (dashed curve) and for glass spheres of radius a in air (dotted curve). The data for all four samples fall on a single smooth curve. This proves that the porous glass is a well-characterized random medium, and also that the light propagation is diffusive. The normalized transport mean free path l^*/λ depends linearly on the size parameter for $a/\lambda \gtrsim 0.3$, as would be expected from the geometrical optics. It is interesting that the linear dependence already appears at a/λ as small as 0.3. With decreasing a/λ, the curve goes through a minimum at $a/\lambda = 0.15$ and turns to increase again. The smallest value $l^*/\lambda \sim 5$, is much larger than the Ioffe-Regel threshold of localization $l^*/\lambda \simeq 1/(2\pi)$. We can therefore safely conclude that the light propagation in the present samples is diffusive in the entire range of size parameter. In the region $a/\lambda \lesssim 0.1$, the curve fits $l^*/\lambda \propto (a/\lambda)^{-3}$ which is expected for Rayleigh scattering by small particles.

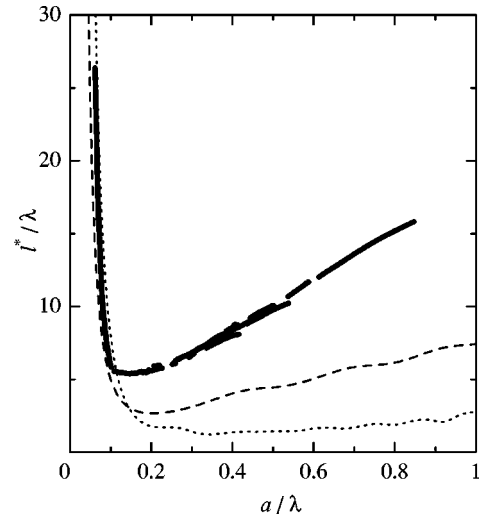

FIG. 2. Size parameter (a/λ) dependence of normalized transport mean free path (l^*/λ) of porous glass. Data for all samples A–D are plotted in the figure (bold curves). The volume fraction of pores is 0.5. The dashed curve and the dotted curve are ISA calculations for spherical holes of radius a in glass and for glass spheres of radius a in air, respectively.

This measurement over a wide range of the size parameter was made possible by combining the transmission spectra of four samples of different pore sizes with a same volume fraction. This is a continuous observation of the crossover of light diffusion from the Rayleigh scattering region to the region of geometrical optics.

B. Time-of-flight measurement and diffusion constant

The diffusion constant D was obtained from the time-of-flight measurement. The surface of the sample plate was irradiated perpendicularly by a cw mode-locked dye laser, and time-resolved total transmission intensity was measured.[21] The wavelength and the autocorrelation width of the dye laser were 603.5 nm and 5 ps, respectively. The transmitted light pulse was detected using a synchroscan streak camera (Hamamatsu Photonics, M1955). The temporal width of the incident pulse observed with the streak camera was 21 ps. In Fig. 3 we show the observed intensity profile of the pulses transmitted through the samples A–D and that of the incident pulse. Also shown in the figure are theoretical curves based on the model of particle diffusion.[32,33] A particle entering a slab of random scattering medium of thickness L at time $t = 0$ on one side undergoes diffusion across the slab to emerge on the other side at time t with the probability per unit time given by

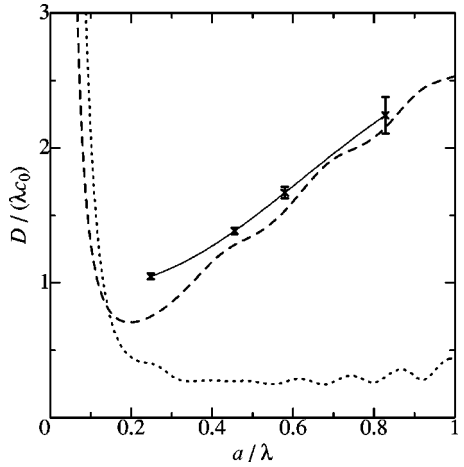

FIG. 4. Size parameter (a/λ) dependence of normalized diffusion constant $[D/(\lambda c_0)]$ of porous glass (bold curve). The volume fraction of pores is 0.5. The dashed curve and the dotted curve are ISA calculations for spherical holes of radius a in glass and for glass spheres of radius a in air, respectively.

$$T(L;t)=\frac{1}{z_0}\frac{D}{(4\pi Dt)^{1/2}}\sum_{n=-\infty}^{\infty}\left[\exp\left(-\frac{[L+2(L+2z_0)n]^2}{4Dt}\right)-\exp\left(-\frac{[L+2(z_p+z_0)+2(L+2z_0)n]^2}{4Dt}\right)\right]. \quad (2.2)$$

The theoretical curves in Fig. 3 are the convolution of Eq. (2.2) with the experimental response function shown at the bottom of the figure, with the parameter D adjusted so as to give the best fit to the measurement. The agreement between the experiment and the theoretical curves is such that one can hardly see the difference. This shows how the long-range behavior of light diffusion in the porous glass is precisely described by the diffusion equation, whereupon yielding the value of D as well.

The same measurement was repeated several times for each sample, changing the irradiation position on the sample surface. The obtained values of D are shown with error bars in Fig. 4 in the dimensionless form $D/(\lambda c_0)$ with c_0 being light velocity in vacuum.

Using the values of l^* and D in the Boltzmann relation

$$D=\frac{1}{3}v_E l^*, \quad (2.3)$$

which is familiar from the standard theory of particle diffusion, we also obtained the transport velocity v_E as a function of a/λ. The result is shown as solid curves in Fig. 5, where it is compared with ISA calculation with the Mie scattering amplitude for spherical holes of radius a in glass (dashed curve), and for glass spheres of radius a in air (dotted curve). The experimentally obtained values of v_E decreases with the increase of the size parameter, approaching $v_E \simeq 0.4c_0$, a value smaller than the light velocity in glass.

Whereas the variation of v_E against a/λ is qualitatively reproduced by the ISA calculation for glass spheres in air, the ISA curve for spherical holes in glass shows opposite dependence on size parameter. For l^* and D, on the other hand, the experimentally obtained values in Figs. 2 and 4 are

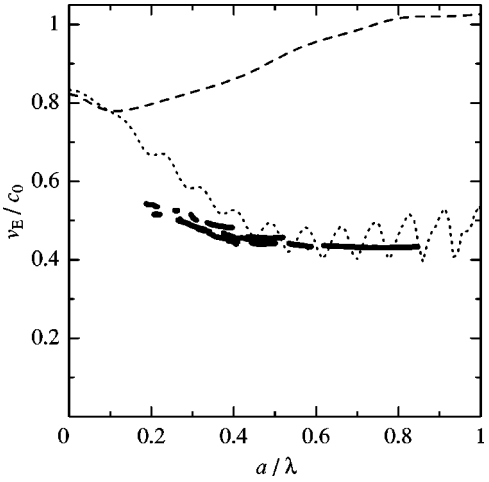

FIG. 5. Size parameter (a/λ) dependence of transport velocity v_E of porous glass (bold curve). Data for all samples A–D are plotted in the figure. The volume fraction of pores is 0.5. The dashed curve and the dotted curve are ISA calculations for spherical holes of radius a in glass and for glass spheres of radius a in air, respectively.

closer to the ISA calculation for spherical holes in glass, and the deviation is significantly larger for the ISA result for glass spheres in air. This contradiction does not appear to be resolved by considering different shapes of scatterers in the ISA calculation, as a similar calculation for long cylindrical scatterers resulted in a similar overall behavior of D and l^* with slightly weaker functional dependence $l^*/\lambda \propto (a/\lambda)^{-2}$ at small a/λ.[21] This is more likely to be an indication of an inherent difficulty of ISA even when applied to the diffusive propagation well away from the Ioffe-Regel criterion of localization.

III. ENERGY DIFFUSION VIA WAVE PROPAGATION

The experimental condition of the previous section invalidates many of the conventional simplifications such as ISA and shell approximation. In the porous glass, the scatterer consists of a randomly connected network of pores whose diameter ranges from 0.05 to 0.85 times λ. The mean free path l is also of the same order as λ, so that the broadening of the wave-vector distribution cannot be ignored. Wave interference effects must be pronounced in such a case, and should introduce a significant modification to the notions based on the model of particle diffusion. In order to examine such wave interference effects, it is necessary to have a theoretical framework that is based squarely on the wave description of energy transport and which has as little recourse as possible to notions borrowed from the particle diffusion model. In this section, we consider, for the sake of simplicity, the propagation of scalar waves in a random medium. We outline the energy transport theory, and derive expressions of such physical quantities as l^*, D, and v_E on a general footing. In the light of this analysis, we then examine the shortcomings of the ISA which is widely used in the literature. The analysis provides the background for the formulation of a model of spatially fluctuating dielectric constant in the next section.

A. Energy current and energy density

In order to discuss the energy transport via wave propagation, expressions of energy density and energy current are required. For a scalar wave propagating among scatterers of a fixed spatial configuration, we start with the Lagrangian

$$L(\nabla\phi,\partial_t\phi,\nabla\phi^*,\partial_t\phi^*;\boldsymbol{r}) \equiv \frac{1}{2}\left[\frac{\varepsilon(\boldsymbol{r})}{c_0^2}\partial_t\phi^*(\boldsymbol{r};t)\partial_t\phi(\boldsymbol{r};t)-\nabla\phi^*(\boldsymbol{r};t)\nabla\phi(\boldsymbol{r};t)\right], \tag{3.1}$$

where ϕ denotes the scalar field, and the ''dielectric constant'' $\varepsilon(\boldsymbol{r})$ is a random function of the spatial coordinates. We do not specify the nature of randomness here, and proceed on a general basis. The energy-momentum tensor

$$T^{\mu}_{\nu}\equiv\frac{\partial L}{\partial\phi_{;\mu}}\phi_{;\nu}+\frac{\partial L}{\partial\phi^*_{;\mu}}\phi^*_{;\nu}-L\,\delta^{\mu}_{\nu}, \quad \mu,\nu,\in t,x,y,z \tag{3.2}$$

then has the form

$$T^t_t=\frac{1}{2}\left[\frac{\varepsilon(\boldsymbol{r})}{c_0^2}\partial_t\phi^*\partial_t\phi+\nabla\phi^*\cdot\nabla\phi\right]$$

and

$$(T^x_t,T^y_t,T^z_t)=-\frac{1}{2}[\partial_t\phi^*\nabla\phi+\nabla\phi^*\partial_t\phi]. \tag{3.3}$$

A scalar wave emitted at time $t=0$ by a point source at a position $\boldsymbol{r}'$ produces an energy current

$$\boldsymbol{j}(\boldsymbol{r},\boldsymbol{r}';\Delta t)\equiv-\frac{1}{2}[\nabla G_+(\boldsymbol{r},\boldsymbol{r}';\Delta t)\partial_t G^*_+(\boldsymbol{r},\boldsymbol{r}';\Delta t) +\nabla G^*_+(\boldsymbol{r},\boldsymbol{r}';\Delta t)\partial_t G_+(\boldsymbol{r},\boldsymbol{r}';\Delta t)] \tag{3.4}$$

at time $t=\Delta t$ at a point $\boldsymbol{r}$, where

$$G_+(\boldsymbol{r},\boldsymbol{r}';\Delta t)=\int\frac{d\boldsymbol{k}}{(2\pi)^3}\int\frac{d\boldsymbol{k}'}{(2\pi)^3}\int\frac{d\omega}{(2\pi)^3}\exp(i\boldsymbol{k}\cdot\boldsymbol{r} -i\boldsymbol{k}'\cdot\boldsymbol{r}')\exp(-i\omega\Delta t)G_+(\boldsymbol{k},\boldsymbol{k}';\omega) \tag{3.5}$$

is the retarded two-point function that satisfies

$$\frac{1}{2}\left[\frac{\varepsilon(\boldsymbol{r})}{c_0^2}\partial^2_{\Delta t}-\nabla^2\right]G_+(\boldsymbol{r},\boldsymbol{r}';\Delta t)=\delta(\Delta t)\,\delta(\boldsymbol{r}-\boldsymbol{r}'). \tag{3.6}$$

The advanced two-point function will be denoted by $G_-(\boldsymbol{r},\boldsymbol{r}';\Delta t)$ or $G_-(\boldsymbol{k},\boldsymbol{k}';\omega)$. Carrying over to the expression in the Fourier space, and taking an average over random realizations of $\varepsilon(\boldsymbol{r})$, the energy current can be written as

$$\boldsymbol{j}(\boldsymbol{r},\boldsymbol{r}';\Delta t)=\int\frac{d\omega}{(2\pi)^3}\int\frac{d\Delta\omega}{(2\pi)^3}\int\frac{d\Delta\boldsymbol{k}}{(2\pi)^3}\exp\{i\Delta\boldsymbol{k}\cdot(\boldsymbol{r}-\boldsymbol{r}') -i\Delta\omega\Delta t\}J(\Delta\boldsymbol{k};\Delta\omega|\omega), \tag{3.7}$$

where

$$\boldsymbol{J}(\Delta\boldsymbol{k};\Delta\omega|\omega)=\frac{1}{2}\int\frac{d\boldsymbol{k}}{(2\pi)^3}[\boldsymbol{k}_+\omega_-+\omega_+\boldsymbol{k}_-]C_{\boldsymbol{k}}(\Delta\boldsymbol{k};\Delta\omega|\omega) \tag{3.8}$$

with $\boldsymbol{k}_\pm=\boldsymbol{k}\pm\frac{1}{2}\Delta\boldsymbol{k}$, and $\omega_\pm=\omega\pm\frac{1}{2}\Delta\omega$. Here,

$$C_{\boldsymbol{k}}(\Delta\boldsymbol{k};\Delta\omega|\omega) \equiv\int\frac{d\boldsymbol{k}'}{(2\pi)^3}\langle G_+(\boldsymbol{k}_+,\boldsymbol{k}'_+;\omega_+)G_-(\boldsymbol{k}_-,\boldsymbol{k}'_-;\omega_-)\rangle_C \tag{3.9}$$

is the sum of Fourier components of the four-point function, and the bracket $\langle\rangle_C$ denotes configurational averaging over the random realizations of $\varepsilon(\boldsymbol{r})$. The quantity $C_{\boldsymbol{k}}(\Delta\boldsymbol{k},\Delta\omega|\omega)$ is the wave-picture equivalent of the probability distribution function of a particle of energy ω that started propagating from a point source in space.

Following the same procedure for the energy density, on the other hand, we arrive at the expression

$$S(\boldsymbol{r},\boldsymbol{r}';\Delta t)\equiv\frac{1}{2}\left\langle\frac{\varepsilon(\boldsymbol{r})}{c_0^2}\partial_t G_+(\boldsymbol{r},\boldsymbol{r}';\Delta t)\partial_t G^*_+(\boldsymbol{r},\boldsymbol{r}';\Delta t) +\nabla G_+(\boldsymbol{r},\boldsymbol{r}';\Delta t)\cdot\nabla G^*_+(\boldsymbol{r},\boldsymbol{r}';\Delta t)\right\rangle_C. \tag{3.10}$$

However, in order to take an average over the random scatterer configurations, information is required of the spatial correlation between the field strength and the dielectric constant $\varepsilon(\boldsymbol{r})$. Therefore, this procedure does not yield an expression of energy density solely in terms of Green's functions.

A way around this problem was proposed by van Albada, van Tiggelen, Lagendijk, and Tip, [24–27] who suggested the use of the Bethe-Salpeter equation for the four-point function. Denoting by $G_{e\pm}$ the two-point function after configurational averaging

$$G_{e\pm}\equiv\langle G_\pm\rangle_C,$$

the four-point function satisfies

$$C_{\boldsymbol{k}}(\Delta\boldsymbol{k};\Delta\omega|\omega) =G_{e+}(\boldsymbol{k}_+;\omega_+)G_{e-}(\boldsymbol{k}_-;\omega_-) \times\left[1+\int\frac{d\boldsymbol{k}_1}{(2\pi)^3}U_{\boldsymbol{k}\boldsymbol{k}_1}(\Delta\boldsymbol{k};\Delta\omega|\omega)C_{\boldsymbol{k}_1}(\Delta\boldsymbol{k};\Delta\omega|\omega)\right], \tag{3.11}$$

where $U_{\boldsymbol{k}\boldsymbol{k}_1}(\Delta\boldsymbol{k};\Delta\omega|\omega)$ is the irreducible scattering kernel.[34–36] Using $G_+G_-=(G_--G_+)/(G_+^{-1}-G_-^{-1})$, this can be recast in the form of a transport equation[3,20]

$$\Delta\omega\left(\frac{\omega}{=}\right)^2 C_{\boldsymbol{k}}(\Delta\boldsymbol{k};\Delta\omega|\omega)-\Delta\boldsymbol{k}\cdot\boldsymbol{k}\omega C_{\boldsymbol{k}}(\Delta\boldsymbol{k};\Delta\omega|\omega)$$

$$=-\omega[G_{e+}(k_+;\omega_+)-G_{e-}(k_-;\omega_-)]\int\frac{d\boldsymbol{k}_1}{(2\pi)^3}U_{\boldsymbol{k}\boldsymbol{k}_1}(\Delta\boldsymbol{k};\Delta\omega|\omega)C_{\boldsymbol{k}_1}(\Delta\boldsymbol{k};\Delta\omega|\omega)+\omega[\Sigma_+(k_+;\omega_+)$$

$$-\Sigma_-(k_-;\omega_-)]C_{\boldsymbol{k}}(\Delta\boldsymbol{k};\Delta\omega|\omega)-\omega[G_{e+}(k_+;\omega_+)-G_{e-}(k_-;\omega_-)], \tag{3.12}$$

where $\Sigma_\pm$ is the self-energy defined by

$$\Sigma_\pm\equiv\overline{G}_\pm^{-1}-G_{e\pm}^{-1}, \tag{3.13}$$

where $\overline{G}_\pm$ is the propagation function for the scatterer-free homogeneous medium with an appropriate uniform dielectric constant $\overline{\varepsilon}=(c_0/c)^2$.

The right-hand side, as it stands, depends implicitly on Δk and $\Delta\omega$ through $k_\pm$ and $\omega_\pm$ in $G_{e\pm}$, $\Sigma_\pm$, and U. However, the dependence on Δk exactly cancels out when $\Delta\omega=0$ due to the Ward-Takahashi (W-T) identity;[37]

$$\Sigma_+(k_+;\omega_+)-\Sigma_-(k_-;\omega_-)=\int\frac{d\boldsymbol{k}_1}{(2\pi)^3}U_{\boldsymbol{k}\boldsymbol{k}_1}(\Delta\boldsymbol{k};\Delta\omega|\omega)[G_{e+}(k_{1+};\omega_+)-G_{e-}(k_{1-};\omega_-)]+\frac{\omega\Delta\omega}{\omega^2+\Delta\omega^2}\Bigg[\Sigma_+(k_+;\omega_+)$$

$$+\Sigma_-(k_-;\omega_-)+\int\frac{d\boldsymbol{k}_1}{(2\pi)^3}U_{\boldsymbol{k}\boldsymbol{k}_1}(\Delta\boldsymbol{k};\Delta\omega|\omega)[G_{e+}(k_{1+};\omega_+)+G_{e-}(k_{1-};\omega_-)]\Bigg]. \tag{3.14}$$

Expanding Eq. (3.12) to first order in $\Delta\omega$ and Δk and integrating over $\boldsymbol{k}$, we obtain

$$\Delta\omega\int\frac{d\boldsymbol{k}}{(2\pi)^3}\left\{\left(\frac{\omega}{=}\right)^2-\left[\mathrm{Re}\,\Sigma_+(k;\omega)+\int\frac{d\boldsymbol{k}_1}{(2\pi)^3}\mathrm{Re}\,G_{e+}(k_1;\omega)\mathrm{Re}\,U_{\boldsymbol{k}_1\boldsymbol{k}}(\boldsymbol{0};0|\omega)\right]\right\}$$

$$\times C_{\boldsymbol{k}}(\Delta\boldsymbol{k};\Delta\omega|\omega)-\omega\int\frac{d\boldsymbol{k}}{(2\pi)^3}(\boldsymbol{k}\cdot\Delta\boldsymbol{k})C_{\boldsymbol{k}}(\Delta\boldsymbol{k};\Delta\omega|\omega)=-i\omega\int\frac{d\boldsymbol{k}}{(2\pi)^3}\mathrm{Im}\,G_{e+}(k;\omega) \tag{3.15}$$

in the limit $\Delta\boldsymbol{k},\Delta\omega\to0$, where the notations Re and Im refer to the real part and the imaginary part, respectively, of a complex quantity. This can be interpreted as an equation of continuity

$$\Delta\omega S-\Delta\boldsymbol{k}\cdot\boldsymbol{J}=iQ \tag{3.16}$$

with the conserved current

$$\boldsymbol{J}=\omega\int\frac{d\boldsymbol{k}}{(2\pi)^3}\boldsymbol{k}C_{\boldsymbol{k}}(\Delta\boldsymbol{k};\Delta\omega|\omega) \tag{3.17}$$

and the conserved density

$$S=\int\frac{d\boldsymbol{k}}{(2\pi)^3}\left\{\left(\frac{\omega}{=}\right)^2-\left[\mathrm{Re}\,\Sigma_+(k;\omega)\right.\right.$$

$$\left.\left.+\int\frac{d\boldsymbol{k}_1}{(2\pi)^3}\mathrm{Re}\,G_{e+}(k_1;\omega)\mathrm{Re}\,U_{\boldsymbol{k}_1\boldsymbol{k}}(\boldsymbol{0};0|\omega)\right]\right\}$$

$$\times C_{\boldsymbol{k}}(\Delta\boldsymbol{k};\Delta\omega|\omega). \tag{3.18}$$

The right-hand side of Eq. (3.15) corresponds to a point source of radiation that is localized both in space and time. Since J coincides with the expression of energy current in Eq. (3.8), S is identified as the energy density in the limit of $\Delta k,\Delta\omega\to0$. The formula (3.18) gives the expression of energy density in terms of the statistical Green's functions alone, with the implication that the wave component of frequency ω and wave number k contributes an amount

$$\gamma_k(\omega)=\left(\frac{\omega}{=}\right)^2-\left[\mathrm{Re}\,\Sigma_+(k;\omega)\right.$$

$$\left.+\int\frac{d\boldsymbol{k}_1}{(2\pi)^3}\mathrm{Re}\,G_{e+}(k_1;\omega)\mathrm{Re}\,U_{\boldsymbol{k}_1\boldsymbol{k}}(\boldsymbol{0};0|\omega)\right] \tag{3.19}$$

to the energy density. It should be noted that formulas (3.8) and (3.18) are independent of any particular approximation scheme.

B. Diffusion parameters

We shall now derive the expressions for diffusion constant, transport mean free path, and transport velocity. As we have seen in the previous section, and as has long been observed, energy propagation in a random medium over a long spatial range and over a long period of time is often diffusive. Energy diffusion then precisely obeys a diffusion equation with a definite diffusion constant D, so that there is no conceptual difficulty in defining D. Using Fick's law

$$\boldsymbol{J} = -iDS\Delta\boldsymbol{k} \tag{3.20}$$

in the limit $\Delta k, \Delta\omega \to 0$, the diffusion constant D is given by

$$D = \lim_{\Delta k,\Delta\omega\to 0} \frac{i\omega \int d\boldsymbol{k}(\boldsymbol{k}\cdot\Delta\boldsymbol{k}) C_{\boldsymbol{k}}(\Delta\boldsymbol{k};\Delta\omega|\omega)}{\int d\boldsymbol{k}\gamma_k(\omega) C_{\boldsymbol{k}}(\Delta\boldsymbol{k};\Delta\omega|\omega)(\Delta k)^2}. \tag{3.21}$$

The transport mean free path l^*, on the other hand, is a microscopic concept, and cannot be determined from the macroscopic long-range behavior of energy density alone. It is then by no means obvious what the precise definition of l^* should be in the wave description of diffusion. Classically, l^* is the spatial range over which a diffusing particle loses its memory of momentum, which may translate into momentum (wave number) correlation length in the wave picture. Here, however, we shall not attempt to give a precise expression to this notion, but instead turn to an analogy with the classical theory of particle diffusion. In the transport theory of elastically scattered classical particles, the particle distribution function has the angular dependence[7,8]

$$C_{\hat{\boldsymbol{k}}}(\Delta\boldsymbol{k};\Delta\omega) \propto \rho(\Delta\boldsymbol{k};\Delta\omega) - il^*\Delta k(\hat{\boldsymbol{k}}\cdot\widehat{\Delta\boldsymbol{k}})\rho(\Delta\boldsymbol{k};\Delta\omega), \tag{3.22}$$

where $\hat{\boldsymbol{k}}$ denotes the unit vector in the direction of $\boldsymbol{k}$, and ρ is the particle density. The transport mean free path l^* appears here as the proportionality coefficient between the degree of anisotropy of momentum distribution and the macroscopic spatial gradient $\nabla\rho/\rho$. Carrying this over to the wave description of diffusion, we shall define the transport mean free path as

$$l^* = \lim_{\Delta k,\Delta\omega\to 0} \frac{3i \int d\boldsymbol{k}\gamma_k(\omega)(\hat{\boldsymbol{k}}\cdot\widehat{\Delta\boldsymbol{k}}) C_{\boldsymbol{k}}(\Delta\boldsymbol{k};\Delta\omega|\omega)}{\int d\boldsymbol{k}\gamma_k(\omega) C_{\boldsymbol{k}}(\Delta\boldsymbol{k};\Delta\omega|\omega)\Delta k}, \tag{3.23}$$

remembering that the wave component $(\omega,\boldsymbol{k})$ contributes an amount $\gamma_k(\omega)$ to the energy density. The presence of the numerical factor may be understood by substituting Eq. (3.22) into Eq. (3.23).

The definition of transport velocity v_{E}, on the other hand, was given by van Tiggelen and co-workers, [24–27] as the coefficient that relates the energy current to the energy distribution anisotropy in the momentum space;

$$J(\Delta k;\Delta\omega|\omega) = v_{\mathrm{E}} \int \frac{d\boldsymbol{k}}{(2\pi)^3}\gamma_k(\omega)(\hat{\boldsymbol{k}}\cdot\widehat{\Delta\boldsymbol{k}}) C_{\boldsymbol{k}}(\Delta\boldsymbol{k};\Delta\omega|\omega). \tag{3.24}$$

Then the transport velocity is

$$v_{\mathrm{E}} = \lim_{\Delta k,\Delta\omega\to 0} \frac{\omega \int d\boldsymbol{k}(\boldsymbol{k}\cdot\widehat{\Delta\boldsymbol{k}}) C_{\boldsymbol{k}}(\Delta\boldsymbol{k};\Delta\omega|\omega)}{\int d\boldsymbol{k}\gamma_k(\omega)(\hat{\boldsymbol{k}}\cdot\widehat{\Delta\boldsymbol{k}}) C_{\boldsymbol{k}}(\Delta\boldsymbol{k};\Delta\omega|\omega)}. \tag{3.25}$$

With the present set of definitions, the Boltzmann relation

$$D = \frac{1}{3} v_{\mathrm{E}} l^*$$

holds between D, l^*, and v_{E}. Let us note that, whereas this relation has long been established for the diffusion of classical particles[7,8] and for wave propagation where a particlelike approximation is valid, the present set of definitions extends its realm of application to the entire diffusive regime of wave propagation.

C. Independent scattering approximation and its problems

The argument of this section has so far been made on general grounds, independent of the particulars of the experimental condition. In order to apply the results to the analysis of an experiment, one is in need of knowledge of the two-point functions and four-point functions appropriate for the experimental condition. However, such knowledge is very rarely available, and one is often compelled to resort to certain simplifying schemes and assumptions as to the behavior of such functions. Widely used in the literature, in this regard, is the ISA, which assumes the wave to be scattered by each scatterer independently of other scatterers and ignores the interference effect of multiple scattering between different scatterers. This approximation is often used in conjunction with the shell approximation, which ignores the broadening of the dispersion relation in the random medium. Both these approximations are valid in the limit of low scatterer density. However, under the experimental condition of the previous section and under a wide range of circumstances where the diffusive propagation of the wave is observed, neither approximation is justified. We have, in fact, seen in the previous section that an analysis based on such a scheme fails to give a consistent account of the observed behavior of l^*, D, and v_{E} as a function of the size parameter. In order to highlight the need for a more comprehensive treatment of multiple scattering effects, let us now analyze the ISA.

In the ISA, one assumes a random medium in which scatterers of a same shape and size are distributed randomly. The two-point function and the four-point function are determined by specifying the self-energy $\Sigma_{\pm}(k;\omega)$ and the irreducible scattering kernel $U_{\boldsymbol{k}\boldsymbol{k}'}(\Delta\boldsymbol{k};\Delta\omega|\omega)$. In the limit of low scatterer density $n_i \simeq 0$, one may retain only the terms of first order in n_i to obtain

$$\Sigma_{\pm}(k;\omega) = n_i t_{i\pm}(\boldsymbol{k},\boldsymbol{k};\omega) \tag{3.26}$$

for the self-energy, and

$$U_{\boldsymbol{k}\boldsymbol{k}'}(\Delta\boldsymbol{k};\Delta\omega|\omega) = n_i t_{i+}(\boldsymbol{k}_+,\boldsymbol{k}'_+;\omega_+) t_{i-}(\boldsymbol{k}_-,\boldsymbol{k}'_-;\omega_-) \tag{3.27}$$

for the scattering kernel, where $t_{i\pm}$ is the retarded/advanced t matrix of the individual scatterer placed alone in a scatterer-free medium. Equations (3.26) and (3.27) represent the ISA.

Now, just as the diffusion pole in particle diffusion results from the particle number conservation, the diffusion pole in the case of energy diffusion results from the energy conservation law. In terms of Green's functions, a conservation law finds its expression in the Ward-Takahashi (W-T) identity [38,39] which plays an important role in determining

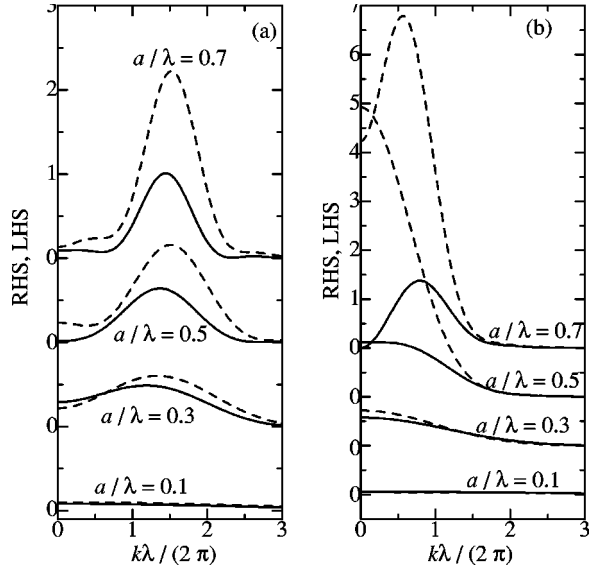

FIG. 6. Comparison between the right-hand side (solid curves) and the left-hand side (dashed curves) of the Ward-Takahashi identity (3.28) for Green's functions in ISA; (a) glass spheres in air, (b) spherical holes in glass.

the behavior of the four-point function near the diffusion pole.[24–27] It is therefore important that the Green's functions satisfy the W-T identity at $\Delta k, \Delta\omega \simeq 0$ in order for the diffusive behavior to be described correctly. In the limit $\Delta k, \Delta\omega \rightarrow 0$, the identity takes the form[26]

$$\mathrm{Im}\,\Sigma_+(k;\omega) = \int \frac{d\boldsymbol{k}_1}{(2\pi)^3} \mathrm{Re}\, U_{\boldsymbol{k}\boldsymbol{k}_1}(\mathbf{0};0|\omega)\, \mathrm{Im}\, G_{e+}(k_1;\omega). \tag{3.28}$$

Substituting Eq. (3.26) and (3.27) into Eq. (3.28), it is seen that the W-T identity is satisfied only up to the first order of $n_i t_i$, since the left-hand side is linear in $n_i t_i$, while

$$G_e = \overline{G} + \overline{G} n_i t_i \overline{G} + \overline{G} n_i t_i \overline{G} n_i t_i \overline{G} + \cdots \tag{3.29}$$

is on the right-hand side. The discrepancy can become large for large values of $n_i t_i \overline{G}(\overline{r})$ where $\overline{r}$ is the typical distance between neighboring scatterers. We compare in Fig. 6 the left-hand side (solid line) and the right-hand side (dotted line) of Eq. (3.28) as functions of k for the case of glass spheres in vacuum [Fig. 6(a)] and for spherical vacuum bubbles in glass [Fig. 6(b)] for various values of size parameter. The dielectric constant of the glass is taken to be $\varepsilon_{\mathrm{glass}} = 2.25$. The discrepancy is significant for $a/\lambda \gtrsim 0.3$.

An immediate remedy for this will be to use the coherent potential approximation[37] and determine the scattering t matrix t_i to be consistent with the coherent potential of the surrounding medium. This, in effect, will partly take into account the interference effect of multiple scattering between a scatterer and other scatterers in its neighborhood. At any rate, comparison of the two sides of Eq. (3.28) shows that it is essential that effects of such interference are taken into account in a consistent description of diffusion at large values of a/λ.

On top of ISA, the shell approximation is often used, sometimes implicitly, in order to simplify integration in the k space[24–27] such as in Eqs. (3.8)–(3.25). This approximation is valid in the limit of dilute scatterers. However, a large value of $\Sigma_\pm(k;\omega)$ under the actual experimental condition invalidates the assumption of small broadening.

To summarize, for the analysis of a wide variety of actual cases of wave diffusion where such simplifying assumptions are invalid, it is necessary to have a scheme that gives a consistent treatment to multiple scattering, and which takes explicit account of the broadening of the Green's functions.

IV. SPATIALLY FLUCTUATING DIELECTRIC CONSTANT MODEL

We shall now take a simple model of a dielectric random medium, and develop a perturbation scheme that satisfies the W-T identity and which also allows inclusion of progressively higher-order effects of multiple scattering. We shall use the scheme to numerically determine two-point functions and four-point functions, and apply the analysis of the previous section to see the short-range interference effect on diffusion. The result will then be compared with the experiment.

A. Gaussian fluctuation model

Electron micrograph shows that the porous glass is a block of glass permeated by a random network of fine pores. It is therefore but a crude approximation to model the medium with a randomly distributed ensemble of spherical scatterers. In fact, attempts to incorporate into ISA the effect of the exclusion volume of the spherical scatterers so that they do not spatially overlap, have invariably resulted in a gross overestimation of l^* at long wavelengths compared to the experiment. This is because there is a local ordering in the spatial configuration of spheres at volume fraction as high as 50%, so that the long-range fluctuation of scatterer density is strongly suppressed. The experimental fact that $l^*/\lambda \propto (a/\lambda)^{-3}$ at long wavelengths suggests that the spatial fluctuation of dielectric constant in a porous glass sample is not as strongly restrained as in a disperse suspension of hard-core scatterers, but is closer to a random fluctuation in space. Considering also the fact that the diffusive behavior of wave propagation is a widely observed phenomenon irrespective of the details of the random medium, we shall make no attempt to model the specific case of the porous glass, but, instead, employ a simple model with a well-controlled fluctuation in space that has a characteristic length scale a to correspond to the pore radius of the porous glass.

The model we employ here is that of a dielectric medium whose dielectric constant $\varepsilon(\boldsymbol{r}) = \overline{\varepsilon} + \Delta\varepsilon(\boldsymbol{r})$ fluctuates randomly around the mean value $\overline{\varepsilon}$ as a function of position $\boldsymbol{r}$. In order to introduce a characteristic length, we assume the fluctuation to have a spatial correlation $g(\Delta\boldsymbol{r}) \equiv \langle \Delta\varepsilon(\boldsymbol{r} + \Delta\boldsymbol{r}) \Delta\varepsilon(\boldsymbol{r}) \rangle_C = \langle \{\Delta\varepsilon(\boldsymbol{r})\}^2 \rangle_C \exp(-(\Delta r)^2/(2a^2))$. To further simplify the model, we also assume that the fluctuation obeys Gaussian statistics, so that all odd-order correlation functions are zero, while all even-order correlation functions can be decomposed into a sum of the products of the two-point correlation functions $g(\Delta\boldsymbol{r})$. In momentum space,

$$\langle \Delta\varepsilon(\boldsymbol{k}) \rangle_C = 0,$$

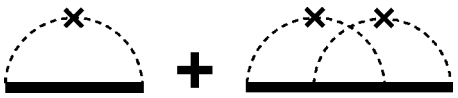

FIG. 7. Self-energy diagrams of the Gaussian fluctuation model.

$$\langle \Delta\varepsilon(\boldsymbol{k}_1)\Delta\varepsilon(\boldsymbol{k}_2)\rangle_C = \delta(\boldsymbol{k}_1-\boldsymbol{k}_2)g(\boldsymbol{k}_1),$$

$$\langle \Delta\varepsilon(\boldsymbol{k}_1)\Delta\varepsilon(\boldsymbol{k}_2)\Delta\varepsilon(\boldsymbol{k}_3)\rangle_C = 0,$$

$$\begin{aligned}\langle \Delta\varepsilon(\boldsymbol{k}_1)\Delta\varepsilon(\boldsymbol{k}_2)\Delta\varepsilon(\boldsymbol{k}_3)\Delta\varepsilon(\boldsymbol{k}_4)\rangle_C &= \delta(\boldsymbol{k}_1-\boldsymbol{k}_2)g(\boldsymbol{k}_1)\delta(\boldsymbol{k}_3-\boldsymbol{k}_4)g(\boldsymbol{k}_3)\\ &+ \delta(\boldsymbol{k}_1-\boldsymbol{k}_3)g(\boldsymbol{k}_1)\delta(\boldsymbol{k}_2-\boldsymbol{k}_4)g(\boldsymbol{k}_2)\\ &+ \delta(\boldsymbol{k}_1-\boldsymbol{k}_4)g(\boldsymbol{k}_1)\delta(\boldsymbol{k}_2-\boldsymbol{k}_3)g(\boldsymbol{k}_2),\ \text{etc.},\end{aligned} \tag{4.1}$$

where $\Delta\varepsilon(\boldsymbol{k})$ and $g(\boldsymbol{k})$ are the Fourier transform of $\Delta\varepsilon(\boldsymbol{r})$ and $g(\boldsymbol{r})$, respectively.

In order to determine the monochromatic two-point function $G_+(\boldsymbol{r},\boldsymbol{r}_0;\omega)$, one has to solve the equation

$$-\frac{1}{2}\left[\left(\nabla^2+\frac{\omega^2}{c_0^2}\bar{\varepsilon}\right)+\frac{\omega^2}{c_0^2}\Delta\varepsilon(\boldsymbol{r})\right]G_+(\boldsymbol{r},\boldsymbol{r}_0;\omega)=\delta(\boldsymbol{r}-\boldsymbol{r}_0). \tag{4.2}$$

Here we regard $\Delta\varepsilon(\boldsymbol{r})$ as the scattering term and apply the standard procedure of the perturbation expansion.[36,40] The property (4.1) of Gaussian fluctuation is particularly convenient for the perturbation calculation of Green's functions. The diagrammatic rule for taking the configurational average is simply to pair up all the scattering vertices, and to assign a value $g(\boldsymbol{q})$ to each pair of vertices that carry a momentum $\boldsymbol{q}$.

In order to obtain the two-point function, one first determines the self-energy $\Sigma_\pm(k;\omega)$, whose two leading terms of perturbation expansion are shown graphically in Fig. 7. The simplest possible approximation is to take only the lowest-order term. However, in order for the W-T identity (3.14) to be satisfied, the choice of approximation must be consistent with the approximation one makes to the irreducible scattering kernel $U_{\boldsymbol{k}\boldsymbol{k}'}(\Delta\boldsymbol{k};\Delta\omega|\omega)$. The perturbation expansion for the scattering kernel is given by such diagrams as in Fig. 8 where we have shown terms of up to second order of scattering. The simplest possible approximation here is to take only the leading term and set

$$U^{(1)}_{\boldsymbol{k}\boldsymbol{k}'}(\Delta\boldsymbol{k};\Delta\omega|\omega)=\left(\frac{\omega_+}{c_0}\right)^2\left(\frac{\omega_-}{c_0}\right)^2 g(|\boldsymbol{k}-\boldsymbol{k}'|). \tag{4.3}$$

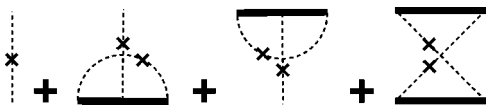

FIG. 8. Scattering kernel diagrams of the Gaussian fluctuation model.

This amounts to making a ladder approximation[36] to the four-point functions, and consistency is achieved only if the self-energy is set equal to the first diagram of Fig. 7 but with $G_{e\pm}(\boldsymbol{k};\omega)$ instead of the unperturbed two-point function $\bar{G}_\pm(\boldsymbol{k};\omega)$ for the internal light propagation line;

$$\Sigma^{(1)}_\pm(\boldsymbol{k}_\pm;\omega_\pm)=\left(\frac{\omega_\pm}{c_0}\right)^4\int\frac{d\boldsymbol{k}_1}{(2\pi)^3}g(|\boldsymbol{k}_\pm-\boldsymbol{k}_1|)G_{e\pm}(k_1;\omega_\pm). \tag{4.4}$$

Since just one scattering center appears in the diagram, we shall hereafter refer to this approximation as the one-site approximation. Although implicit account is taken of the multiple scattering between different scattering centers by solving Eqs. (4.3), (4.4), (3.13), and (3.11) self-consistently, one notices that no cross-interference terms such as the second diagram of Fig. 8 are included in this approximation. In contrast to ladder diagrams, such crossed diagrams represent interference between time-reversed paths, and are known to play an important role in Anderson localization.[34,35,41] In particular, the collection of maximally crossed diagrams is known to produce precursor effects of localization such as the backscattering peak.[42,43] For our samples, the observed backscattering peak has an angular width of a few tens of milliradians.[21] Since it occupies only 0.01% of the entire solid angle, the energy flow involved in the interference of high orders of multiple scattering is small in magnitude at distances beyond l^*. Nevertheless, low-order effects should be present at short distances and affect the quantities such as l^*, D, and v_E.

In order to see such effects of cross interference, we shall consider a second type of approximation. If one wishes to add the cross-interference diagram to the one-site scattering kernel, other terms also need be added in order to preserve consistency with the W-T identity. The smallest set of diagrams is then given by the entire set of diagrams in Figs. 7 and 8, so that

$$\Sigma^{(2)}_\pm(\boldsymbol{k}_\pm;\omega_\pm)=\Sigma^{(1)}_\pm(\boldsymbol{k}_\pm;\omega_\pm)+\left(\frac{\omega_\pm}{c_0}\right)^4\left(\frac{\omega_\pm}{c_0}\right)^4\int\frac{d\boldsymbol{k}_1}{(2\pi)^3}\int\frac{d\boldsymbol{k}_2}{(2\pi)^3}g(|\boldsymbol{k}_\pm-\boldsymbol{k}_1|)g(|\boldsymbol{k}_\pm-\boldsymbol{k}_2|)$$

$$\times G_{e\pm}(k_1;\omega_\pm)G_{e\pm}(k_2;\omega_\pm)G_{e\pm}(|\boldsymbol{k}_1+\boldsymbol{k}_2-\boldsymbol{k}_\pm|;\omega_\pm) \tag{4.5}$$

for the self-energy, and

$$U^{(2)}_{\boldsymbol{k}\boldsymbol{k}'}(\Delta\boldsymbol{k};\Delta\omega|\omega)=U^{(1)}_{\boldsymbol{k}\boldsymbol{k}'}(\Delta\boldsymbol{k};\Delta\omega|\omega)+\left(\frac{\omega_+}{c_0}\right)^4\left(\frac{\omega_-}{c_0}\right)^4\int\frac{d\boldsymbol{k}_1}{(2\pi)^3}g\left(\left|\frac{1}{2}(\boldsymbol{k}-\boldsymbol{k}')-\boldsymbol{k}_1+\frac{1}{2}\Delta\boldsymbol{k}\right|\right)g\left(\left|\frac{1}{2}(\boldsymbol{k}-\boldsymbol{k}')+\boldsymbol{k}_1-\frac{1}{2}\Delta\boldsymbol{k}\right|\right)$$
$$\times G_{\mathrm{e}+}\left(\left|\frac{1}{2}(\boldsymbol{k}+\boldsymbol{k}')+\boldsymbol{k}_1\right|;\omega_+\right)G_{\mathrm{e}-}\left(\left|\frac{1}{2}(\boldsymbol{k}'+\boldsymbol{k})-\boldsymbol{k}_1\right|;\omega_-\right)+\left(\frac{\omega_-}{c_0}\right)^2\left(\frac{\omega_+}{c_0}\right)^6\int\frac{d\boldsymbol{k}_1}{(2\pi)^3}g(|\boldsymbol{k}-\boldsymbol{k}'|)$$
$$\times g\left(\left|\frac{1}{2}(\boldsymbol{k}+\boldsymbol{k}')-\boldsymbol{k}_1+\frac{1}{2}\Delta\boldsymbol{k}\right|\right)G_{\mathrm{e}+}\left(\left|\frac{1}{2}(\boldsymbol{k}-\boldsymbol{k}')+\boldsymbol{k}_1\right|;\omega_+\right)G_{\mathrm{e}+}\left(\left|\frac{1}{2}(\boldsymbol{k}'-\boldsymbol{k})+\boldsymbol{k}_1\right|;\omega_+\right)$$
$$+\left(\frac{\omega_+}{c_0}\right)^2\left(\frac{\omega_-}{c_0}\right)^6\int\frac{d\boldsymbol{k}_1}{(2\pi)^3}g(|\boldsymbol{k}-\boldsymbol{k}'|)g\left(\left|\frac{1}{2}(\boldsymbol{k}+\boldsymbol{k}')-\boldsymbol{k}_1-\frac{1}{2}\Delta\boldsymbol{k}\right|\right)G_{\mathrm{e}-}\left(\left|\frac{1}{2}(\boldsymbol{k}-\boldsymbol{k}')+\boldsymbol{k}_1\right|;\omega_-\right)$$
$$\times G_{\mathrm{e}-}\left(\left|\frac{1}{2}(\boldsymbol{k}'-\boldsymbol{k})+\boldsymbol{k}_1\right|;\omega_-\right) \tag{4.6}$$

for the irreducible scattering kernel. Since two scattering centers appear in the diagrams, we shall hereafter refer to this approximation as the two-site approximation. (A similar set of diagrams was used within shell approximation by van Tiggelen and Lagendijk[44] in the analysis of wave diffusion among point scatterers in terms of resonantly induced dipole-dipole interactions.) For later reference, we shall name the third term and the last two terms in Fig. 8, cross graph and ψ graphs, respectively, after their appearance.

B. Numerical procedure

Once the set of diagrams for the self-energy and the irreducible scattering kernel have been specified, the Dyson equation (3.13) and the Bethe-Salpeter equation (3.11) can be solved self-consistently for $\Sigma_\pm(k;\omega)$ and $C_{\boldsymbol{k}}(\Delta\boldsymbol{k};\Delta\omega|\omega)$. In order to deal squarely with the broadening of the dispersion relation in the random medium, we solve for $\Sigma_\pm(k;\omega)$ and $C_{\boldsymbol{k}}(\Delta\boldsymbol{k};\Delta\omega|\omega)$ explicitly as functions of momentum $\boldsymbol{k}$.

First, Eqs. (4.4) or (4.5) is solved for $\Sigma_\pm(k;\omega)$ iteratively by calculating $G_{\mathrm{e}\pm}(k;\omega)=\{\overline{G}_\pm(k;\omega)-\Sigma_\pm(k;\omega)\}^{-1}$ from tentative values of $\Sigma_\pm(k;\omega)$ and substituting the result on the right hand side to obtain the next approximation to $\Sigma_\pm(k;\omega)$. Once the convergence has been achieved, the result for $G_{\mathrm{e}\pm}(k;\omega)$ is then used in Eq. (3.11) and either one of Eq. (4.3) and Eq. (4.6) to be solved for $C_{\boldsymbol{k}}(\Delta\boldsymbol{k};\Delta\omega|\omega)$.

Here we introduce a simplification, since we need to know the behavior of $C_{\boldsymbol{k}}(\Delta\boldsymbol{k};\Delta\omega|\omega)$ only in the limit $\Delta\boldsymbol{k},\Delta\omega\to 0$. Considering the fact that $C_{\boldsymbol{k}}(\Delta\boldsymbol{k};\Delta\omega|\omega)$ has a diffusion pole at $\Delta\boldsymbol{k}=\boldsymbol{0},\Delta\omega=0$, we shall set

$$C_{\boldsymbol{k}}(\Delta\boldsymbol{k};\Delta\omega|\omega)=\frac{2\pi^2}{\Delta\omega+D\Delta k^2}\{\alpha_k(\omega)+3(\hat{\boldsymbol{k}}\cdot\widehat{\Delta\boldsymbol{k}})\beta_k(\omega)\}. \tag{4.7}$$

Substituting this into the Bethe-Salpeter equation (3.11), one finds that $\alpha_k(\omega)$ and $\beta_k(\omega)$ satisfy

$$\alpha_k(\omega)=|G_{\mathrm{e}+}(k;\omega)|^2\int\frac{k_1^2dk_1}{2\pi^2}U_{kk_1}(\omega)\alpha_{k_1}(\omega), \tag{4.8}$$

$$\beta_k(\omega)-3|G_{\mathrm{e}+}(k;\omega)|^2\int\frac{k_1^2dk_1}{2\pi^2}U_{k_{\Delta k}k_{1\Delta k}}(\omega)\beta_{k_1}(\omega)$$
$$=i\int\frac{k_1^2dk_1}{2\pi^2}\left[\left|G_{\mathrm{e}+}(k;\omega)\right|^2\mathrm{Im}\frac{\partial U_{kk_{1\Delta k}}(\omega)}{\partial\Delta k}\right.$$
$$\left.+\frac{1}{3}\mathrm{Im}\left\{\frac{\partial G_{\mathrm{e}+}(k;\omega)}{\partial k}G_{\mathrm{e}-}(k;\omega)\right\}U_{kk_1}(\omega)\right]\alpha_{k_1}(\omega)\Delta k, \tag{4.9}$$

where

$$U_{kk_1}(\omega)\equiv\int\frac{d\Omega_k}{4\pi}\int\frac{d\Omega_k}{4\pi}U_{\boldsymbol{k}\boldsymbol{k}_1}(\boldsymbol{0};0|\omega),$$

$$U_{k_{\Delta k}k_{1\Delta k}}(\omega)\equiv\int\frac{d\Omega_k}{4\pi}\int\frac{d\Omega_k}{4\pi}U_{\boldsymbol{k}\boldsymbol{k}_1}(\boldsymbol{0};0|\omega)(\hat{\boldsymbol{k}}\cdot\widehat{\Delta\boldsymbol{k}})(\hat{\boldsymbol{k}}_1\cdot\widehat{\Delta\boldsymbol{k}}),$$

$$\frac{\partial U_{kk_{1\Delta k}}(\omega)}{\partial\Delta k}\equiv\int\frac{d\Omega_k}{4\pi}\int\frac{d\Omega_k}{4\pi}\frac{\partial U_{\boldsymbol{k}\boldsymbol{k}_1}(\boldsymbol{0};0|\omega)}{\partial\Delta\boldsymbol{k}}\cdot\Delta\hat{\boldsymbol{k}}(\hat{\boldsymbol{k}}_1\cdot\widehat{\Delta\boldsymbol{k}}). \tag{4.10}$$

From Eq. (4.8), we see that $\alpha_k(\omega)$ is the eigenfunction of the scattering kernel with the eigenvalue 1. In reality, the kernel has only one eigenvalue in the neighborhood of 1 and all other eigenvalues are small in comparison, so that the amount of deviation from unity of the computed value of the largest eigenvalue provides a good consistency check of the numerical procedure. We found that the deviation could always be made small by increasing the number of mesh points for the representation of $\Sigma_\pm(k;\omega)$ in the $\boldsymbol{k}$ space. The fact that the largest eigenvalue is unity, in fact, derives from the energy conservation law, and is related to the W-T identity. Multiplying both sides of Eq. (3.14) by $G_{\mathrm{e}+}(k_+;\omega_+)G_{\mathrm{e}-}(k_-;\omega_-)$ and setting $\Delta k,\Delta\omega=0$, one obtains

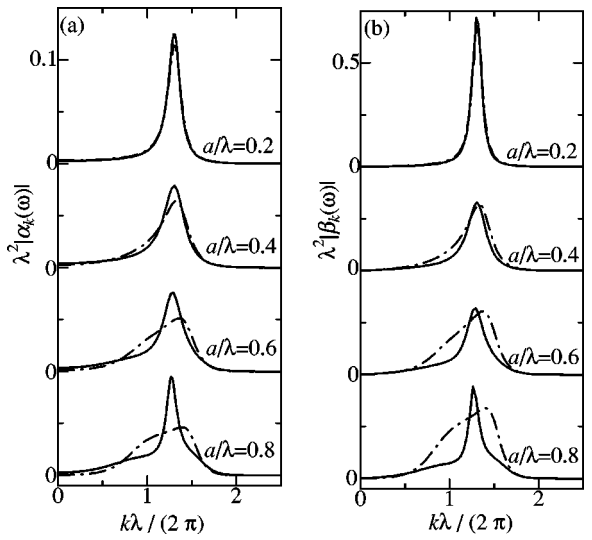

FIG. 9. Normalized distribution functions (a) $\lambda^2|\alpha_k|$ and (b) $\lambda^2|\beta_k|$ for various values of the size parameter a/λ calculated for the spatially fluctuating dielectric constant model. The dot-dash line is the one-site approximation, and the solid line is the two-site approximation.

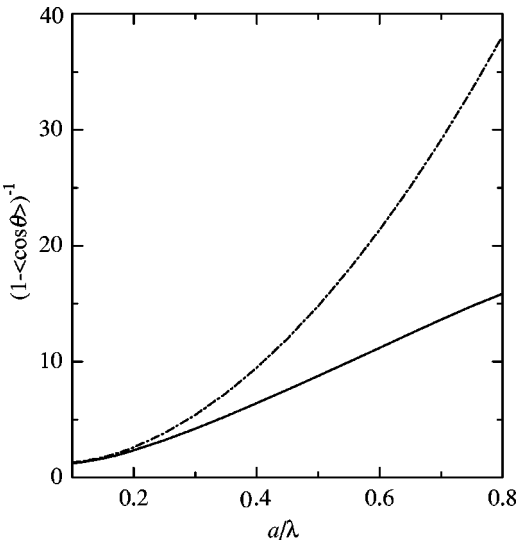

FIG. 10. Size parameter dependence of $1/(1-\langle\cos\theta\rangle)$ for the spatially fluctuating dielectric constant model, where $\langle\cos\theta\rangle$ is the index of forward scattering as defined in Eq. (4.13) of the text. The dot-dashed curve is the one-site approximation, and the solid curve is the two-site approximation.

$$\mathrm{Im}\, G_{e+}(k;\omega)=|G_{e+}(k;\omega)|^2\int\frac{k_1^2dk_1}{2\pi^2}\times U_{kk_1}(\omega)\,\mathrm{Im}\, G_{e+}(k_1;\omega). \quad (4.11)$$

Comparing this with Eq. (4.8), one concludes that α_k is proportional to Im $G_{e+}(k;\omega)$, so that no new calculation is required for α_k. The physical reason for this equivalence is that, since $\alpha_k(\omega)$ is the equilibrium distribution function in the momentum space at $t\to\infty$ for a monochromatic wave that started at a point in space at $t=0$, it must be identical to the density of states Im $G(k;\omega)$ of the monochromatic wave of frequency ω.

For $\beta_k(\omega)$, on the other hand, there is no similar relationship with two-point functions, so that it has to be determined from the Bethe-Salpeter equation (4.9). The equation is linear in $\beta_k(\omega)$, and can be readily solved once $\alpha_k(\omega)$ has been determined. We here note that, as far as l^*, D, and v_E are concerned, we need not determine the overall normalization factor for $C_{\boldsymbol{k}}(\Delta\boldsymbol{k};\Delta\omega|\omega)$ [see Eqs. (3.21), (3.23), and (3.25)].

In the actual numerical calculation, we divided the momentum space into a finite number (up to 160) of thin concentric spherical shells, and determined values of $\Sigma_{\pm}(k;\omega)$, $\alpha_k(\omega)$, and $\beta_k(\omega)$ on each shell, assuming they were constant within a shell.

C. Numerical results

In Fig. 9 we show $\alpha_k(\omega)$ and $\beta_k(\omega)$ as functions of k for several values of size parameter a/λ and for the two types of approximation. Here, the amplitude of dielectric constant fluctuation is set so as to correspond to porous glass samples;

$$\langle\Delta\varepsilon^2(\boldsymbol{r}_C)\rangle_C\equiv\langle\varepsilon^2\rangle_C-\overline{\varepsilon^2}=f(1-f)(\varepsilon_{\mathrm{air}}-\varepsilon_{\mathrm{glass}})^2=0.39, \quad (4.12)$$

where we have used $f=0.5$, $\varepsilon_{\mathrm{air}}=1.0$, and $\varepsilon_{\mathrm{glass}}=2.25$.

In the one-site approximation, the peak in $\alpha_k(\omega)\propto$Im $G_{e+}(k;\omega)$ is sharp for small values of size parameter ($a/\lambda\lesssim 0.2$). However, at $a/\lambda\simeq 0.4$, the peak width becomes comparable to the central wave number, confirming *a posteriori* the necessity for a full treatment of the wave number broadening. In the two-site approximation, the peak is noticeably narrower than in the one-site approximation for large values of a/λ. Although this result appears to justify the use of shell approximation for a wider range of size parameter than is expected from the Fermi's golden rule, it should be noted that the justification is made only by carrying out a calculation that allows description of broadening. It is also unclear from the present result alone whether inclusion of higher order terms will not overturn the result of the two-site approximation. Inspection of the contribution from each term in Eq. (4.5) reveals that the two-site term oscillates rapidly as a function of k near $k\simeq 2\pi\sqrt{\overline{\varepsilon}}/\lambda$, resulting in a significant reduction of $\Sigma_{\pm}(k;\omega)$ compared to the one-site approximation near the on-shell momentum $k\simeq 2\pi\sqrt{\overline{\varepsilon}}/\lambda$.

In order to see the dependence of scattering kernel $U_{\boldsymbol{kk}'}$ on the scattering angle θ between $\boldsymbol{k}$ and $\boldsymbol{k}'$, we define the index of forward scattering $\langle\cos\theta\rangle$ as the ratio of the forward scattering (Y_1^0) component to the isotropic (Y_0^0) component of $U_{\boldsymbol{kk}'}$;

$$\langle\cos\theta\rangle\equiv\frac{\int d\boldsymbol{k}\alpha_k\int d\boldsymbol{k}'\,\alpha_k'U_{\boldsymbol{kk}'}(\omega)(\hat{\boldsymbol{k}}\cdot\hat{\boldsymbol{k}}')}{\int d\boldsymbol{k}\alpha_k\int d\boldsymbol{k}'\,\alpha_k'U_{\boldsymbol{kk}'}(\omega)}. \quad (4.13)$$

Following an analogy with the classical theory of particle diffusion where the relation $l^*=l(1-\langle\cos\theta\rangle)^{-1}$ holds between the transport mean free path and the scattering mean free path, we plot in Fig. 10 the factor $(1-\langle\cos\theta\rangle)^{-1}$ as a function of a/λ for the two types of approximation. For the one-site approximation, the scattering is directed increas-

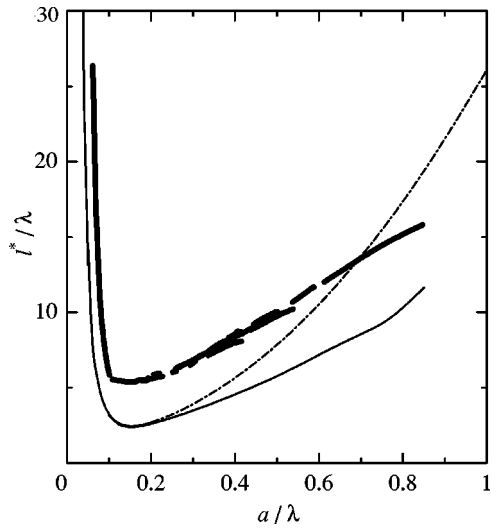

FIG. 11. Size parameter (a/λ) dependence of normalized transport mean free path (l^*/λ) for spatially fluctuating dielectric constant model. The dot-dashed curve is the one-site approximation, and the solid curve is the two-site approximation. The bold curve is the experiment for porous glass.

ingly in the forward direction as the size parameter is increased, so that $\langle \cos\theta \rangle$ grows monotonically to approach unity leading to large values of $(1-\langle \cos\theta \rangle)^{-1}$ at large a/λ. For the two-site approximation, the anisotropy is smaller in the entire range of the size parameter, resulting in a significant reduction of $(1-\langle \cos\theta \rangle)^{-1}$ compared to the one-site approximation at large a/λ. As a consequence, the transport mean free path l^* is smaller in the two-site approximation than in the one-site approximation in the entire range of a/λ, despite the fact that the momentum distribution width is narrower so that the scattering mean free path is longer in the two-site approximation.

The transport mean free path l^* and the diffusion constant D calculated with the full expressions (3.23) and (3.21) are

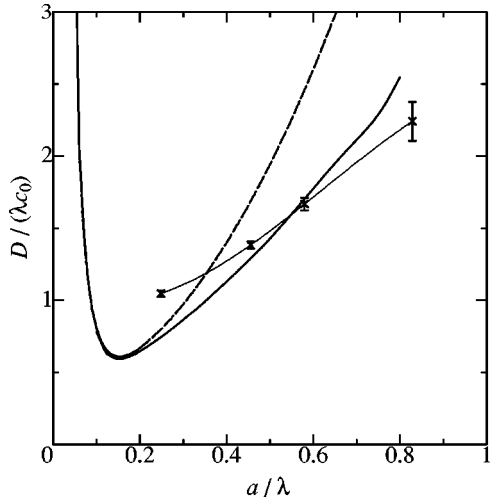

FIG. 12. Size parameter (a/λ) dependence of normalized diffusion constant $[D/(\lambda c_0)]$ of spatially fluctuating dielectric constant model. The dot-dashed curve is the one-site approximation, and the solid curve is the two-site approximation. The bold curve is the experiment for porous glass.

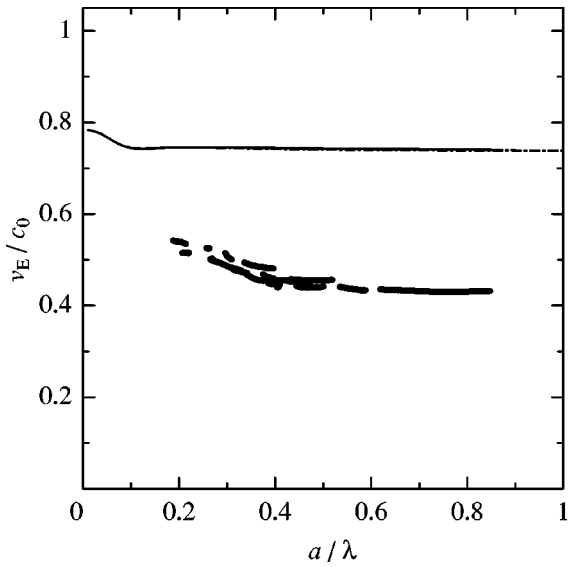

FIG. 13. Size parameter (a/λ) dependence of transport velocity v_E of spatially fluctuating dielectric constant model. The dot-dashed curve is the one-site approximation, and the solid curve is the two-site approximation. The bold curves are the experiment for porous glass.

shown in Figs. 11 and 12 together with the experimental data. There is an improvement in the a/λ dependence when the two-site effect is included. This can be regarded as a manifestation of the interference effect of multiple scattering through the reduction of forward scattering. The present result does not show the oscillatory resonance behavior seen in ISA calculations that use Mie scattering t matrix of spheres of a fixed radius [21,32,45–48]. This is because we now consider random fluctuation of dielectric constant with Gaussian spatial correlation, so that such sharp structures as are associated with Mie scattering are smeared out. A spherical scatterer is known to have very large Q values at large values of size parameter [45,46] because of the high symmetry of the sphere. The present perturbative treatment does not take full account of multiple scattering within a single scatterer, which may also be the reason for the lack of structure in the present calculation. However, in modeling light diffusion in such a medium as porous glass with the volume fraction approaching 50%, the random network structure should make such one-site multiple-scattering effects relatively unimportant.

The result for v_E is compared with the experiment in Fig. 13. There is little difference between the two types of approximation. A detailed inspection reveals that the cross graph in Eq. (4.6) works to slow down v_E, but the effect is almost exactly counterbalanced by the contribution from the ψ graphs. The physics behind this cancellation is as yet unclear, and may be related to the conservation law and the W-T identity. Nevertheless, the net effect of scattering is that the transport velocity is a decreasing function of a/λ, as was the case in the experiment, and contrary to the result of ISA for spherical holes in glass.

There are several possible causes of deviation of the calculation from the experiment. The truncation of perturbation expansion is the largest source of ambiguity, which will be remedied only by a calculation that includes higher-order terms of multiple scattering. While the contribution of high-

order diagrams is expected to be small in the diffusive regime where interference effects are confined largely within the spatial distance of l^*, three-site and four-site scattering terms may significantly alter the results of two-site approximation for large values of a/λ. Another possible source of deviation is the neglect of the vector nature of electromagnetic waves in the present calculation. It is possible to reformulate the present calculation so as to include the polarization effect along the same line as was done for the backscattering calculation by MacKintosh and John.[49] Since the polarization should match for waves to interfere, the net result should be a reduction of interference as was the case for backscattering.

While keeping such limitations in mind, we may regard the two-site approximation to be in better qualitative agreement with the experiment than the one-site approximation, and a significant improvement over the ISA which fails to give even a qualitative account of the size parameter dependence observed in the experiment. We also note that there is no adjustable parameter in the present calculation. The difference between one-site and two-site approximation results points to the importance of interference effects in the diffusion regime when the size parameter is large, and also in a wide variety of situations where wave energy diffusion is observed.

V. CONCLUSIONS

The measurements of transmission spectra and temporal profile of the transmitted pulse from porous glass are well explained by the diffusion model of light propagation. By curve fitting, we obtained the size parameter dependence of l^* and D. Size parameter dependence of v_E was obtained from l^* and D by using the Boltzmann relation $D = v_E l^*/3$. This is the first continuous observation of the crossover from the Rayleigh scattering region to the region of geometrical optics in a random scattering medium. Although the transport mean free path is much larger than the Ioffe-Regel threshold in the present porous glass samples, the obtained values of l^*, D, and v_E cannot be consistently explained by the ISA. Therefore we derived general expressions of l^*, D, and v_E on a footing beyond the shell approximation or ISA by considering the wave nature of multiple light scattering, and obtained the Boltzmann relation in this framework. Moreover, by using the model of spatially correlated dielectric constant fluctuation, we obtained the theoretical curves whose size-parameter dependence agrees with the experimentally obtained values of l^*, D, and v_E. The difference between one-site and two-site approximation results indicates the importance of interference effects even in the diffusion regime. The quantitative deviation in v_E might be resolved by taking into account the higher-order interference effects than the two-site approximation.

*Present address: Institute of Laser Engineering, Osaka University, 2-6 Yamadaoka, Suita, Osaka 565, Japan. Electronic address: skawato@ile.osaka-u.ac.jp

[1] P. W. Anderson, Philos. Mag. B **52**, 505 (1985).
[2] S. John, Phys. Today **44** (5), 32 (1991).
[3] P. Sheng, *Scattering and Localization of Classical Waves in Random Media* (World Scientific, Singapore, 1990).
[4] A. Ishimaru, *Wave Propagation and Scattering in Random Media* (Academic, New York, 1978), Vols. 1, 2.
[5] S. Chandrasekhar, *Radiative Transfer* (Dover, New York, 1960).
[6] P. A. Lee and T. V. Ramakrishnan, Rev. Mod. Phys. **57**, 287 (1985).
[7] J. R. Lamarsh, *Introduction to Nuclear Reactor Theory* (Addison-Wesley, Reading, MA, 1966).
[8] J. J. Duderstadt, *Nuclear Reactor Analysis* (Wiley, New York, 1976).
[9] A. F. Ioffe and A. R. Regel, Prog. Semicond. **4**, 237 (1960).
[10] B. L. Al'tshuler and P. A. Lee, Phys. Today **41** (12), 36 (1988).
[11] S. John, H. Sompolinsky, and M. J. Stephen, Phys. Rev. B **27**, 5592 (1983).
[12] S. John and M. J. Stephen, Phys. Rev. B **28**, 6358 (1983).
[13] S. John, Phys. Rev. Lett. **53**, 2169 (1984).
[14] S. M. Cohen and J. Machta, Phys. Rev. Lett. **54**, 2242 (1985).
[15] T. R. Kirkpatrick, Phys. Rev. B **31**, 5746 (1985).
[16] C. A. Condat and T. R. Kirkpatrick, Phys. Rev. B **32**, 495 (1985).
[17] M. P. van Albada and A. Lagendijk, Phys. Rev. Lett. **55**, 2692 (1985).
[18] P. E. Wolf and G. Maret, Phys. Rev. Lett. **55**, 2696 (1985).
[19] L. Tsang and A. Ishimaru, J. Opt. Soc. Am. A **1**, 836 (1984).
[20] P. Sheng, *Introduction to Wave Scattering, Localization and Mesoscopic Phenemena* (Academic, San Diego, 1995).
[21] S. Kawato, T. Hattori, T. Takemori, and H. Nakatsuka, Phys. Rev. B **49**, 90 (1994).
[22] D. S. Wiersma, P. Bartolini, A. Lagendijik, and R. Righini, Nature (London) **390**, 671 (1997).
[23] Y. Kuga and A. Ishimaru, J. Opt. Soc. Am. A **1**, 831 (1984).
[24] B. A. van Tiggelen, Ph.D. thesis, University of Amsterdam, 1992.
[25] M. P. van Albada, B. A. van Tiggelen, A. Lagendijk, and A. Tip, Phys. Rev. Lett. **66**, 3132 (1991).
[26] B. A. van Tiggelen, A. Lagendijk, M. P. van Albada, and A. Tip, Phys. Rev. B **45**, 12 233 (1992).
[27] A. Lagendijk and B. A. van Tiggelen, Phys. Rep. **270**, 143 (1996).
[28] *MPG - Micro Porous Glass Catalogue*, Asahi Glass Ltd., Tokyo.
[29] P. W. Atkins, *Physical Chemistry*, 4th ed. (Oxford University Press, Oxford, 1990).
[30] T. H. Elmer, I. D. Chapman, and M. E. Nordberg, J. Phys. Chem. **67**, 2219 (1963).
[31] N. Garcia, A. Z. Genack, and A. A. Lisyansky, Phys. Rev. B **46**, 14 475 (1992).
[32] G. H. Watson, Jr., P. A. Fleury, and S. L. McCall, Phys. Rev. Lett. **58**, 945 (1987).
[33] J. M. Drake and A. Z. Genack, Phys. Rev. Lett. **63**, 259 (1989).
[34] D. Vollhardt and P. Wölfle, Phys. Rev. B **22**, 4666 (1980).
[35] D. Vollhardt and P. Wölfle, Phys. Rev. Lett. **45**, 842 (1980).
[36] G. D. Mahan, *Many-Particle Physics*, 2nd ed. (Plenum, New York, 1990).
[37] J. Kroha, C. M. Soukoulis, and P. Wölfle, Phys. Rev. B **47**, 11 093 (1993).
[38] J. C. Ward, Phys. Rev. **78**, 182 (1950).
[39] Y. Takahashi, Nuovo Cimento **6**, 371 (1957).
[40] G. Richayzen, *Green's Functions and Condensed Matter* (Academic, London, 1984).
[41] D. E. Khmel'Nitsukii, Physica B **126**, 235 (1984).
[42] L. Tsang and A. Ishimaru, J. Opt. Soc. Am. A **2**, 1331 (1985).

[43] E. Akkermans, P. E. Wolf, and R. Maynard, Phys. Rev. Lett. **56**, 1471 (1986).
[44] B. A. van Tiggelen and A. Lagendijk, Phys. Rev. B **50**, 16 729 (1994).
[45] H. C. van de Hulst, *Light Scattering by Small Particles* (Dover, New York, 1981).
[46] C. F. Bohren and D. R. Huffman, *Absorption and Scattering of Light by Small Particles* (Wiley, New York, 1983).
[47] E. Kogan and M. Kaveh, Phys. Rev. B **46**, 10 636 (1992).
[48] G. Cwilich and Y. Fu, Phys. Rev. B **46**, 12 015 (1992).
[49] F. C. MacKintosh and S. John, Phys. Rev. B **37**, 1884 (1988).